Pergamon

Int. J. Multiphase Flow Vol. 22, No. 2, pp. 239–258, 1996

0301-9322(95)00081-X
0301-9322/96 $15.00 + 0.00

WAKE-INDUCED RELATIVE MOTION OF BUBBLES RISING IN LINE

J. KATZ and C. MENEVEAU
Department of Mechanical Engineering, Johns Hopkins University, Baltimore, MD 21218, U.S.A.

(Received 27 July 1995; in revised form 26 November 1995)

Abstract—The motion of nearly spherical air bubbles rising in a column in stagnant water is measured at Reynolds numbers ranging from $Re_D = 0.2$ to 35. The relative velocity is found to be dependent on the distance between bubbles and on their diameter. For the larger bubbles, the relative velocities increased with decreasing distance, reaching maximum values just prior to contact. For the smaller bubbles, the relative velocity decreased prior to coalescence. For the entire range of Reynolds numbers considered, the wake-induced relative motion results in collisions between bubbles. These collisions culminate in coalescence at the present levels of water purity and surface tension. In order to understand the basic features of the measured relative motion, a simple model is developed. It is based on the known flow field and viscous-wake structure around a single bubble, and examines how other bubbles move within this field. Oseen flow for $Re \ll 1$ and potential flow with a thin wake for $Re \gg 1$ are assumed. The approximations involved limit the validity of the model to distances larger than a few bubble diameters. The general agreement between the predictions and experimental results suggest that the model contains the most relevant mechanisms that govern the interaction, within its range of validity. Prior analyses for non-deformable bubbles that predicted an equilibrium distance due to balance between pressure gradients and wake-induced motion, are contradicted by the observed coalescence. A possible cause for the discrepancy is bubble deformation.

Key Words: bubbles, coalescence, wake, bubbly flow

1. INTRODUCTION

Extensive literature is already devoted to the interaction between bubbles rising in a liquid. The case of lateral approach in potential flows has been considered, for example, by van Wijngaarden (1983) and Kok (1989). Several models of bubble cloud dynamics, all of which are based on potential flow interactions only, have subsequently been developed (e.g. Sangani & Didwania 1993). Although viscous effects can be accounted for in a limited sense by including the drag on the bubble, these models do not contain wakes and their effects on other bubbles. Pairs of bubbles rising in-line within such a flow field are predicted to repel each other vertically, and only attract each other horizontally. Simulations of bubble clouds have shown that this leads to horizontal layers of bubbles (Sangani & Didwania 1993). This phenomenon is not observed in practice, possibly because of the effects of viscous wakes that are not included in the potential flow model.

For a single pair of bubbles rising in line, Harper (1970) included a thin wake in an otherwise potential flow analysis, and predicted the existence of an equilibrium distance, at which the adverse pressure gradient balances the wake-induced relative motion. Yuan & Prosperetti (1994) reached the same conclusion in a recent numerical study of the relative motion of a spherical bubble pair. Experimentally, however, collisions of a trailing bubble induced by the wake of the leading one has been observed in numerous studies, which are mainly reported in the chemical engineering literature (e.g. Nevers 1971; Crabtree & Bridgwater 1971; Narayanan *et al.* 1974; Hills 1975, etc.). The majority of these studies deal with highly deformed spherical cap bubbles, typically large air bubbles in water at high Reynolds numbers. The data for smaller Reynolds numbers are obtained in other fluids, but at Eötvös numbers ($Eo = g\rho D^2/\sigma$) much larger than unity, which means that the bubbles are also quite deformed. To the best of our knowledge, there are no experimental data on the wake-induced motion of nearly spherical bubbles, such as air bubbles in water, at Reynolds numbers between 0.2 and 100, and Eötvös numbers of less than 0.3. The present study addresses these flow conditions, both experimentally and by developing a simple model for the relative motion.

This work focuses on the mechanisms that cause bubbles to approach each other due to viscous wake interactions, but not on the fine details of collision and/or coalescence when the two bubbles are very close. The coalescence process when the distance between bubbles is very small, where film-thinning, bubble deformation and surface contaminants are important, has been studied in Chesters & Hofman (1982), Kok (1993) and Tsao & Koch (1994). These studies have shown that if the water is sufficiently pure, coalescence may follow film thinning, slight bubble deformation and film rupture. The present experimental results exhibit such coalescence after in-line approach of the trailing bubble, as long as the water is sufficiently pure.

The paper is organized as follows. The first part (section 2), contains experimental results. It addresses several issues: (a) observation of approach, bubble collision and coalescence of bubbles of equal size over a wide range of Reynolds numbers; (b) illustration of typical interactions between bubbles of different sizes; (c) observations on non-typical interactions; and (d) quantification of the relative velocity as function of the relative distance between approaching bubble pairs, parameterized with the Reynolds number. In the second part (section 3) we apply simple wake models to predict the relative motion of bubbles rising in a column. These models are based on the expected flow structure around a bubble and its wake, at different Reynolds numbers. Section 4 contains a discussion of the results and the conclusions.

2. A COLUMN OF AIR BUBBLES RISING IN WATER: EXPERIMENTS

2.1. Setup

A schematic description of the experimental setup is presented in figure 1. For most of the experiments, the bubbles were injected into a square, 15 cm wide and 1 m long, vertical, transparent chamber, filled with commercially available distilled water. The injectors were manufactured by stretching 1 mm glass capillary tubes under heat, until a nozzle with a typical exit diameter ranging between 10 and 50 μm was formed. Pressure regulators and a fine metering valve were used for controlling the air flux. Based on experience gained in previous studies (Ran & Katz 1991), this nozzle could generate a uniform train of bubbles with diameters ranging between 50 and 1000 μm

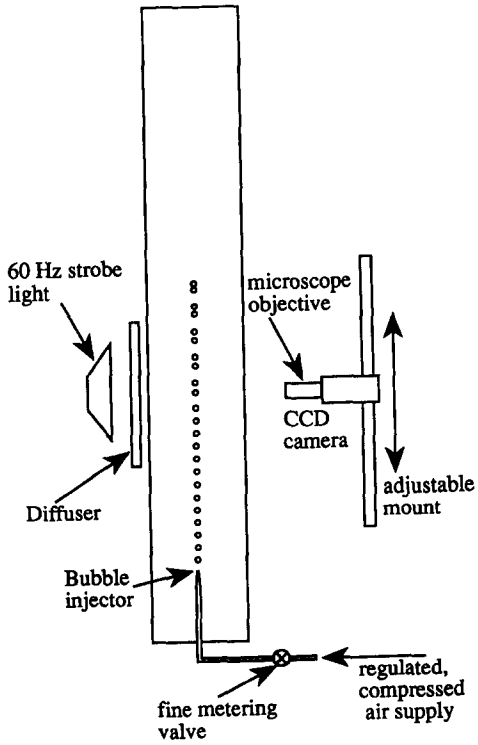

Figure 1. A schematic description of the experimental setup.

without special difficulties. The variation (twice the standard deviation) in bubble size prior to coalescence has been consistently less than 1.5%, which was, at least for the smaller bubbles, also our optical resolution limit. Silhouette images were recorded with a CCD camera connected with a SVHS recorder, and by illuminating the chamber with a 60 Hz strobotac. The bubble size was determined prior to and after each experiment at a high magnification in order to insure that no changes occurred during the run.

The displacements and distance between bubbles were determined at much lower magnifications, typically at levels that kept the same bubble within the field of view for at least 5–7 frames. Images were recorded at several elevations, starting from the injector up to the point where several coalescences, and the resulting differences in rise velocity, disrupted the column. During analysis the images were digitized, and relevant sections from successive video frames were sliced and combined into a single array. The strobe was pulsed at 60 Hz in order to generate independent images in each field (two interlaced fields create a single frame), but only the first field was digitized from each frame. Typical images, composed from a series of successive video frames, are presented in figure 2(a) and (b). The first displays a uniform column following injection, but prior to any

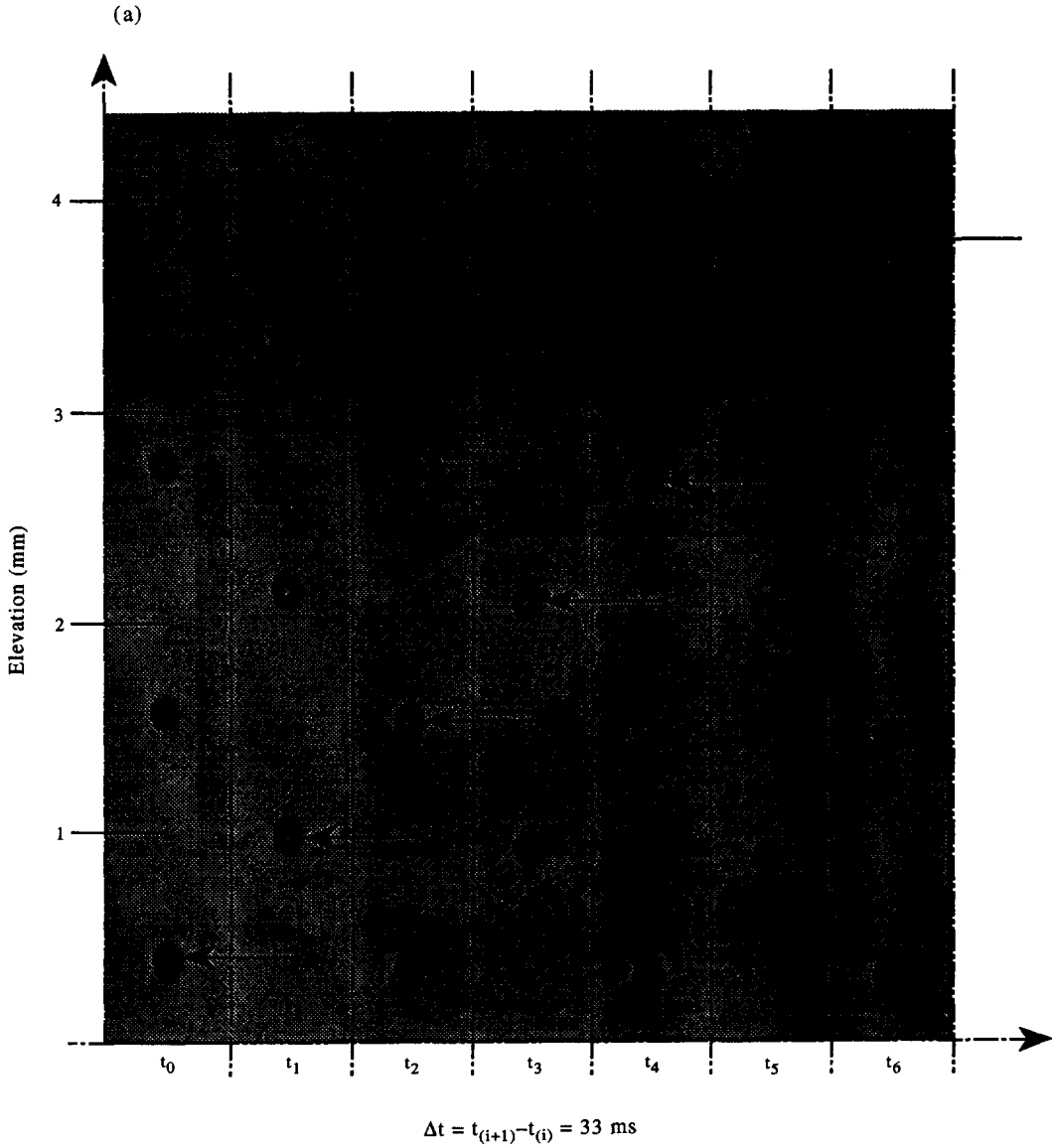

Figure 2(a). *Caption on p. 242.*

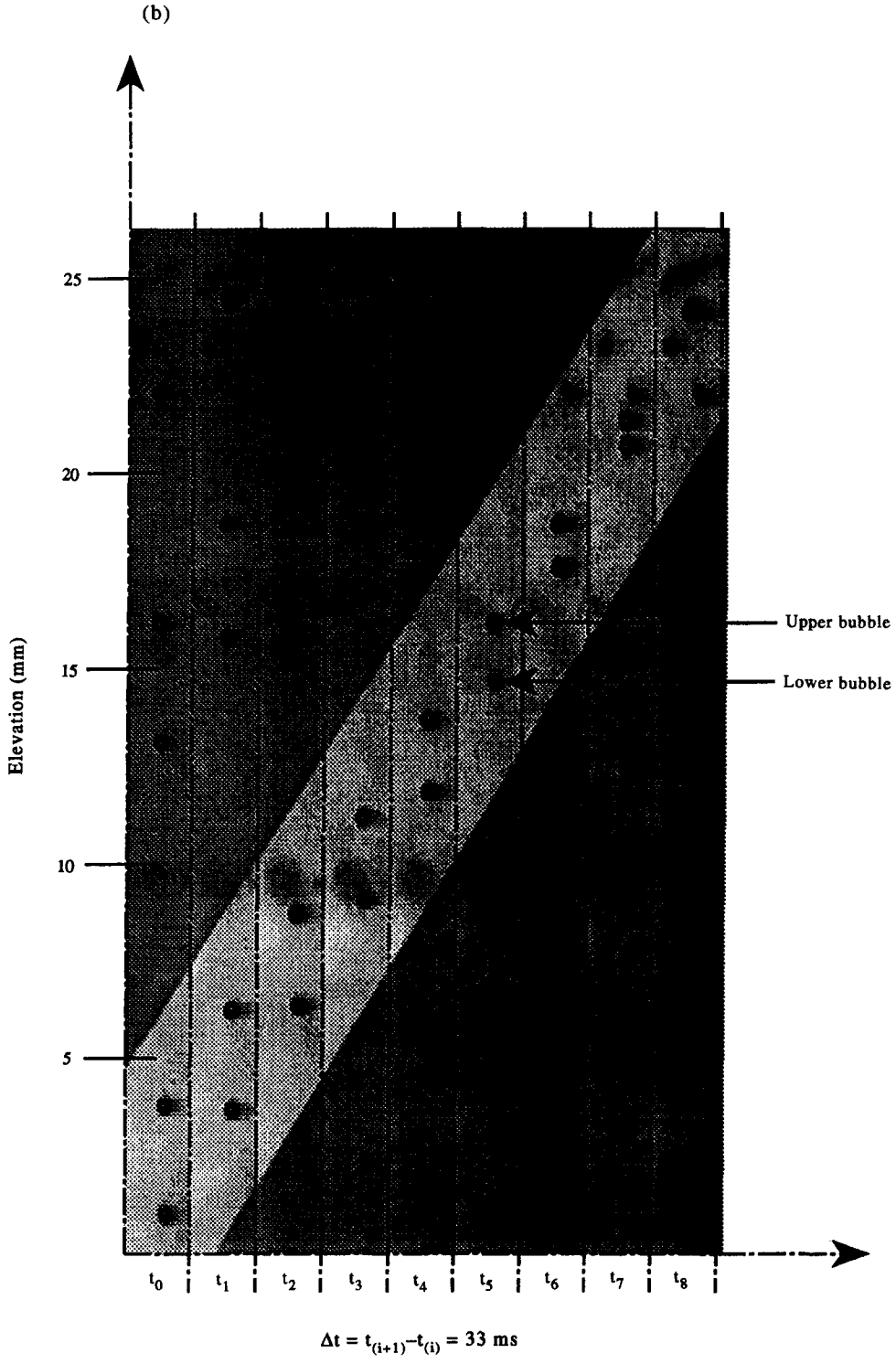

Figure 2(b).

Figure 2. (a) A uniform column of 158 μm diameter bubbles. The image is created by consolidating seven successive video frames. The arrows point at the same bubble; (b) a combined sequence of video frames demonstrating the coalescence of two 475 μm diameter bubbles.

wake-induced relative motion. The second image displays the coalescence of a pair of 475 μm diameter bubbles.

As noted before, the experiments were performed in commercially available distilled water, without any additional treatment. We chose to start with such water and not with highly purified liquid, since it is impractical to use the latter in large scale facilities—where cavitation and multiphase flow tests are performed. The purity of the water was sufficient to insure coalescence of bubbles as they approached each other vertically. Bouncing of bubbles, which can occur when surface contaminants inhibit film rupturing (see, for example, Kok 1989), or when surface tension is very high, never occurred. Nevertheless, to insure that our results are robust with respect to increased purity of water, we have repeated some of the experiments in pure water—filtered with a Milli-Q50 filtering system, that provided resistivity of 18 MΩ cm and surface tension of 72.4 dyne/cm at 22°C.

2.2. Typical and atypical interactions

A series of sample photographs illustrating the interaction between 158 μm bubbles is presented in figure 3(a)–(d). The first shows the most commonly occurring phenomenon, namely relative motion and subsequent coalescence of a pair of bubbles with the same diameter. Such coalescence was observed for bubble sizes ranging from 69 to 800 μm (Reynolds numbers between 0.2 and 140). In figure 3(b) a pair of 158 μm bubbles coalesce, and then the consolidated 199 μm bubble coalesces with another bubble of similar size. We remark that the elongated shape of the coalesced bubble seen in figure 3(b) is a highly transient phenomenon. The bubble becomes spherical a very short time thereafter. We succeeded in maintaining two generations of coalescence for almost the entire column when we started with 69 μm bubbles that coalesced to 87 μm bubbles and then coalesced

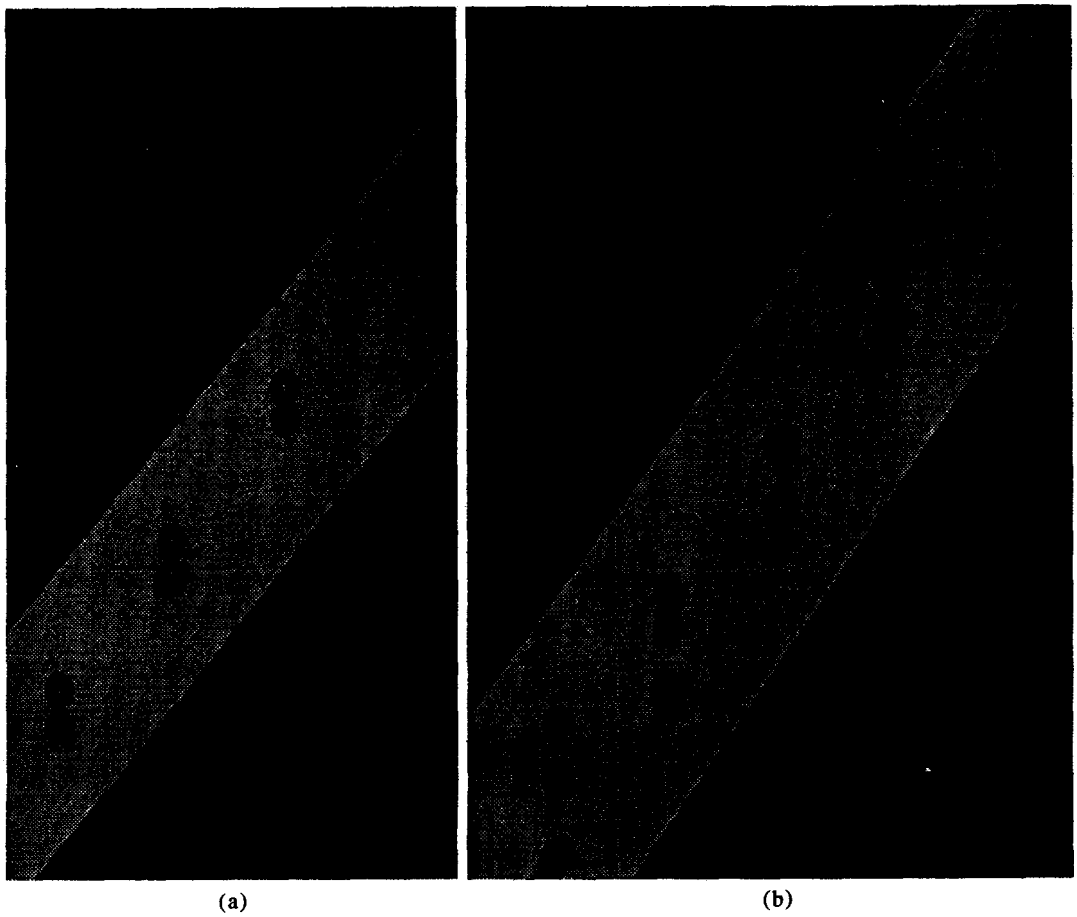

(a) (b)

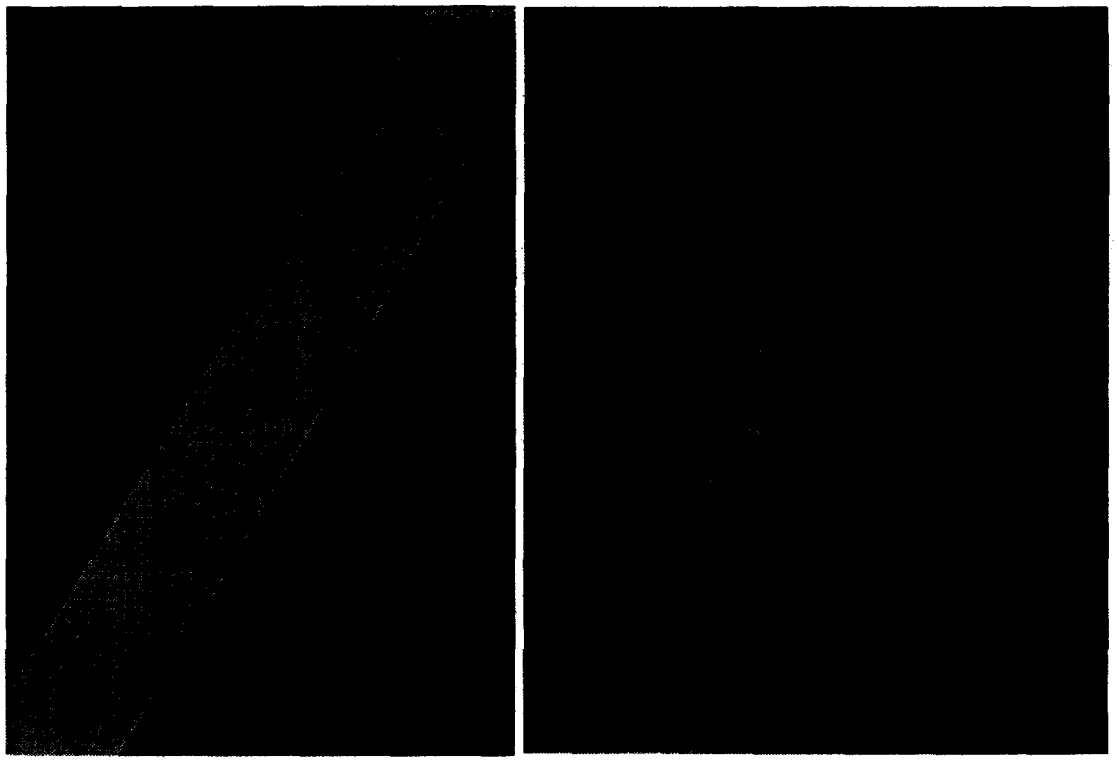

Figure 3. (c), (d).

Figure 3. Images demonstrating observed bubble interactions. Scales are the same as in figure 3(a). (a) coalescence of 158 μm bubbles; (b) formation of a 199 μm bubble and its coalescence with another bubble of the same size; (c) misaligned bubbles of different sizes do not coalesce; and (d) aligned bubbles of different size may coalesce.

again. With 158 μm bubbles, we were successful only part of the time. Coalescence of the larger bubbles (349 and 475 μm) already involved substantial disruption to the column, and in most cases the bubbles became misaligned. Once coalescence started occurring it was possible to examine interactions between bubbles of different sizes. Since the larger bubble moved at a higher velocity, eventually it ran into a smaller bubble. We found that if the train was misaligned by about one half of the larger bubble radius, bubbles of different sizes did not coalesce, as is demonstrated in figure 3(c) (although it is possible that they would have coalesced in purer water—this issue is beyond the scope of the present study). Rejection of small bubbles by large spherical cap bubbles has been observed before (e.g. Hills 1975). When the misalignment in the column was less than about 20% ($\pm 10\%$) of the larger radius, even bubbles with different diameter coalesced [figure 3(d)]. The above-mentioned accuracy of threshold misalignment is due to resolution limitations during the coalescence experiments (the bubble size was determined at about 10 times this magnification, but the area covered in such an image covered only a very small area around the bubble).

2.3. Measurement of bubble velocities

Displacements and distances between bubbles were measured by selecting two small sections of the image enclosing the desired bubbles, and cross-correlating them. The correlation function, $C(x_0, y_0)$, is defined as:

$$C(x_0, y_0) = \sum_{i=0}^{n_i} \sum_{j=0}^{n_i} I(x_i, y_j) I(x_i - x_0, y_j - y_0), \qquad [1]$$

where $I(x_i, y_j)$ is the gray level of a pixel located at (x_i, y_j) (measured consistently from the same origin). The displacements were determined from the locations of the correlation peaks. For most

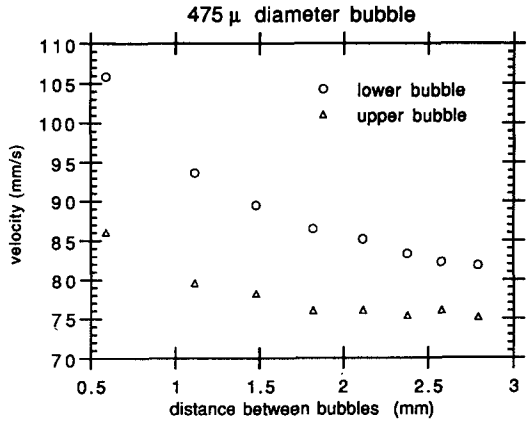

Figure 4. Rise velocities of a pair of coalescing 475 μm diameter bubbles. Data are determined from the images presented in figure 2(b).

cases we were only interested in the vertical displacement. Further improvement in accuracy was achieved by interpolating between the discrete values of $C(x_0, y_0)$, provided that the image size was sufficiently large. Based on error analysis and calibration experiments described in Dong *et al.* (1992) and Sridhar & Katz (1995), the maximum resolution for the present experiments was in the order of 0.1–0.2 pixels. Considering that the displacement between bubbles varied between 0 and 80 pixels, the error was, for most cases, below 1%. The velocity was determined by dividing the displacement of a bubble by the delay between video frames (1/30 s). A typical plot showing the velocities of both bubbles during the coalescence process, as a function of the distance between them, is presented in figure 4. The data were calculated from the image presented in figure 2(b).

2.4. Results

The behavior of bubbles at five different diameters: 69, 87, 158, 349 and 475 μm was investigated in detail during the present study. The qualitative phenomena illustrated in the sample photographs (figures 2 and 3) occurred in all five cases. The "terminal velocities" of these bubbles, namely the rise velocities when the column was uniform, are plotted in figure 5, along with terminal velocities of bubbles having Stokes flow or Levich drag coefficients (see, for example, Clift *et al.* 1978). Other sizes included in this graph are obtained from bubbles formed as a result of coalescence. The range of Reynolds numbers Re = 0.20 to 56 covers several flow regimes, ranging from the Stokes/Oseen to the boundary layer/thin wake flows. In all cases the bubbles remained close to a spherical shape until just prior to coalescence. The results clearly show that the terminal velocity is close to predictions based on Stokes flow at low Reynolds numbers and gradually approaches the Levich equation. We remark, however, that the measured terminal velocity of the

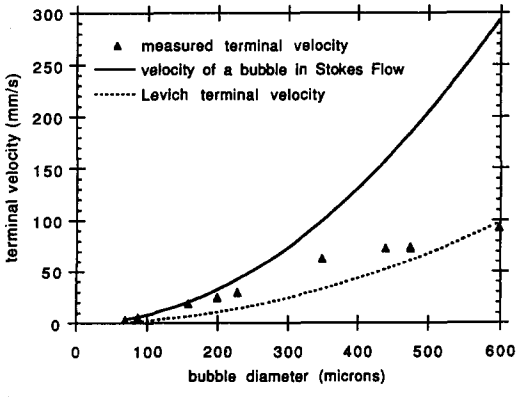

Figure 5. Measured rise velocities of bubbles when the column is uniform (prior to coalescence).

598 μm diameter bubble is very close to the Levich prediction, even though one would expect significant deviations coming from the Moore correction at this Reynolds number (Re = 56). Slight water impurities or bubble deformation could be the cause (we have not attempted to elucidate the precise cause for this result, since the 598 μm bubbles are not among those for which detailed velocity measurements are performed in this study).

Rise velocities (absolute and relative) of approaching bubbles, plotted against the distance between them, are presented in figures 6–9. In two cases (69 and 87 μm bubbles—figure 6), we actually follow the very same pair. In fact, both data sets were recorded during the same run, in which 69 μm bubbles were injected, coalesced and formed a train of 87 μm bubbles (exactly double the volume). In order to cover the entire process it was necessary to record the images at lower magnifications and the results are slightly less accurate (5%). In all the other cases (figures 7–9) the magnifications are similar to figures 2 and 3, and the plots contain data obtained from 20 to 40 bubble pairs. Each pair provides 4–7 data points, such as figure 4. As is evident from the results, data obtained at different elevations and initial spacing still collapse quite well onto clearly defined lines, that depend only on the instantaneous spacing and the bubble diameter. Thus, it is reasonable to assume that the process is quasi-steady in nature, i.e. the bubble velocity depends only on its instantaneous distance from its neighboring bubble, and not on its time history. This assumption is utilized in the second part of this paper.

Several trends can be observed from the results. For separations exceeding two bubble diameters, the relative velocity gradually increases with decreasing distance between bubbles. At smaller separations, the trends depend on bubble diameter. The relative velocities of 349 and 475 μm bubbles reach maximum values just prior to contact, implying that coalescence occurs rather abruptly. Clearly, the wake-induced relative motion is sufficiently powerful to overcome any reaction force caused by pressure gradients. As noted before, collision and coalescence occurred

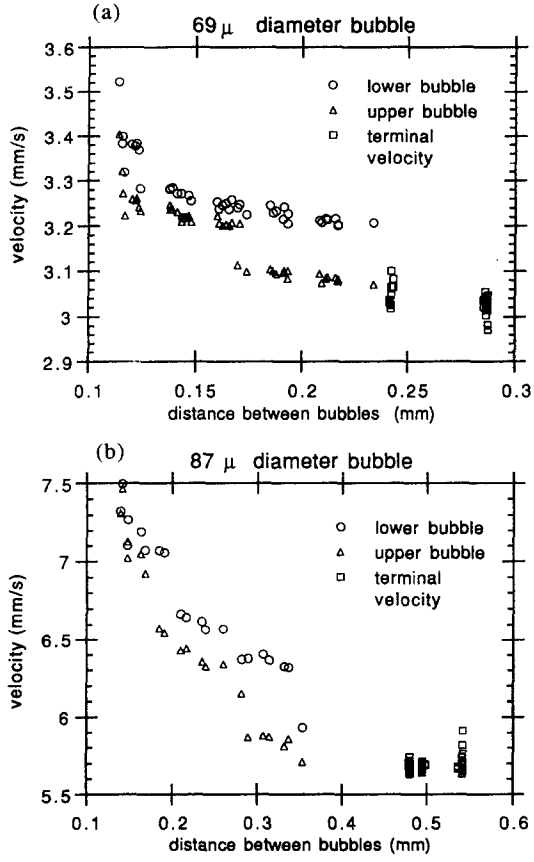

Figure 6. Rise velocities of a coalescing pair of (a) 69 μm diameter bubbles and (b) 87 μm diameter bubbles. The "terminal" velocities are obtained from other bubbles.

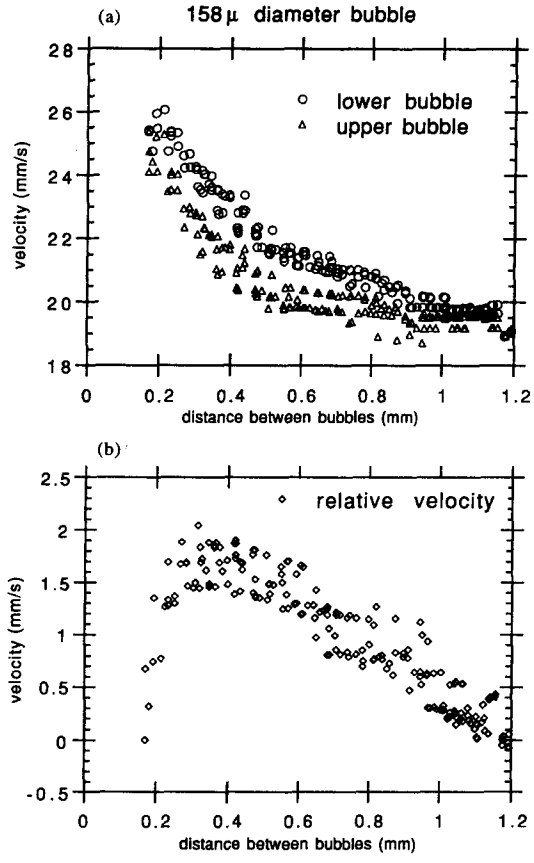

Figure 7. (a) Rise velocities of coalescing pairs of 158 μm diameter bubbles and (b) the corresponding relative velocities.

with 800 μm diameter bubbles as well. This is not the case for the smaller bubbles (69, 87 and 158 μm). Their relative velocities are maximum when the distances between them are 2–2.5 diameters. In fact, the relative motion is slowed down considerably prior to coalescence, and each pair tends to move together for a while, slowly reducing the distance between the two bubbles (possibly due to film thinning), until coalescence finally occurs. This phenomenon is made especially clear by the "kink" in the velocity of the upper bubble in figure 6 (when the distance is 0.17 and 0.27 mm for the 69 and 87 μm diameter bubbles, respectively), and to a lesser extent from figure 7(b).

Another trend related to bubble size is the behavior of the upper bubble. In the case of 349 and 475 μm diameters, the upper bubble is not affected significantly by the presence of the lower bubble until the distance between them becomes smaller than 3–4 diameters. The only effect is a slight decrease in the velocity of the upper bubble as they start forming approaching pairs. As will be discussed later, this phenomenon occurs due to an increasing distance of the upper bubble from the pair above it, which reduces the wake-induced velocity of the fluid surrounding it. In the case of the smaller bubbles (158, 67 and 87 μm), the upper bubble is "pushed" by the lower one for the entire range of distances between bubbles, which for the 158 μm bubbles exceeds 6 diameters. Causes for this trend will be discussed in the following section.

When the distance between the smaller bubbles is less than twice their size and they move together, their velocity is almost equal to the terminal velocity of the coalesced bubble. For example, the velocity of a pair of 158 μm bubbles is near 26 mm/s [see figure 7(a)], and the terminal speed of a 199 μm bubble is about 28 mm/s [see figure 5]. On the other hand, the velocities of the lower 349 and 475 μm bubbles exceed the terminal speeds of the corresponding coalesced bubbles. For example, the terminal speeds of 440 and 598 μm bubbles are 73 and 93 mm/s, respectively, much lower than 83 and 108 mm/s, the corresponding maximum speed of the lower 349 and 475 μm

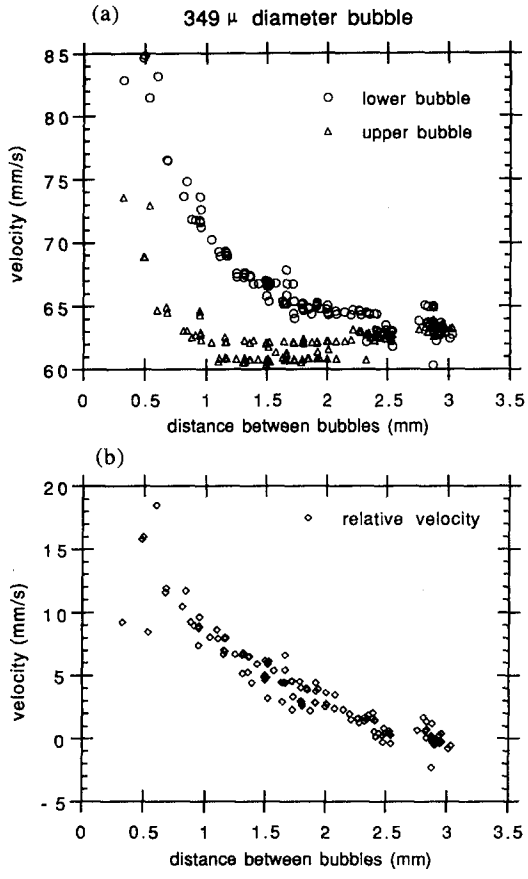

Figure 8. (a) Rise velocities of coalescing pairs of 349 μm diameter bubbles and (b) the corresponding relative velocities.

bubbles. However, in both cases prior to coalescence the upper bubble moves at the terminal speed of the coalesced pair.

3. COMPARISON WITH SIMPLE MODEL

The goal of this section is to ascertain if the measured approach velocities of the bubbles (until they are a few diameters apart), can be reproduced by simple models, which are based on the flow structure around a single bubble.

3.1. Basic assumptions

Instead of considering the complete two (or multiple)-bubble problem, we use the known structure of the flow around a single bubble and consider how other bubbles move within this flow field. This approximation is acceptable when bubbles are far apart. The second approximation is to replace the entire column of bubbles by a series of bubble pairs (see figure 10), and to use periodicity in the analysis. A justification for this assumption will be provided below. We first focus on interactions between bubbles within a pair. Interactions of the upper bubble with the pair above it, and that of the lower bubble with the pair underneath it, are evaluated using periodic boundary conditions. The initial spacing between bubbles is called λ_0, and the period employed in the calculation is $2\lambda_0$. Inherent to our model, the initially uniform column is unstable. Once the distance between two bubbles decreases slightly (for any reason) the velocity of the lower bubble increases until an inevitable collision. There is no "restoring force" that can force the bubble back to the original gap, λ_0. As will be shown shortly, a possible repulsive force due to pressure gradients is weak, except for small distances at high Reynolds numbers. As the velocity of the lower bubble

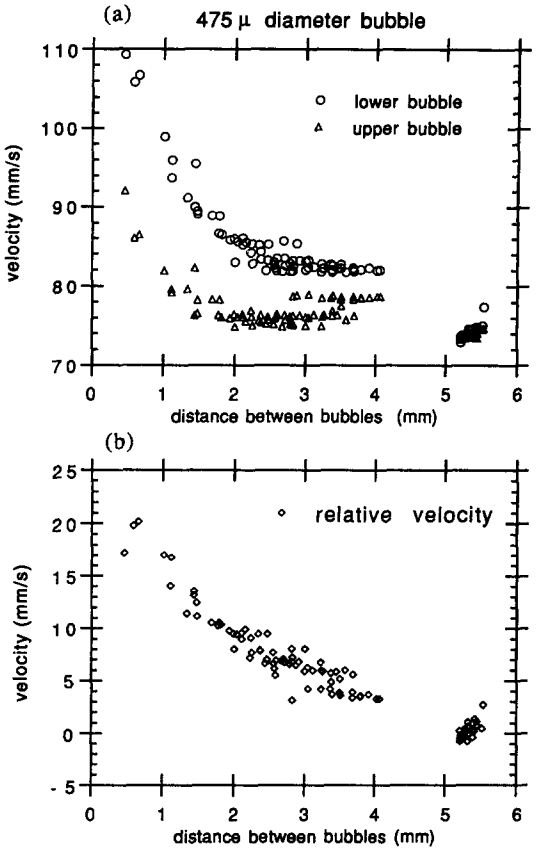

Figure 9. (a) Rise velocities of coalescing pairs of 349 μm diameter bubbles and (b) the corresponding relative velocities.

increases, its distance from a third bubble below it increases, which slows this third bubble. As a result its distance from a fourth bubble decreases. Thus, slow-down of a single bubble starts a process that divides the entire column into a series of bubble pairs. This process was evident in most of the experiments, and in some cases, after the pairs coalesced, it was possible to follow the approach and coalescence process of the second "generation". These observations support modeling the column as a series of periodically spaced bubble pairs (see figure 10).

The forces acting on each bubble include buoyancy, drag due to relative motion within the surrounding fluid, and the dynamic pressure gradient. Note that the latter two effects are induced by both the bubbles above and below. The assumption of quasi-equilibrium is made throughout, so that time-dependent effects are neglected. This assumption is consistent with the experimental results since the acceleration is very low, and the rise velocity seems to depend only on the distance between bubbles, and not on their time history. Two limiting regimes, $\mathrm{Re} \ll 1$ and $\mathrm{Re} \gg 1$ are considered, in the hope of capturing bounds for the intermediate Reynolds number regime prevalent in the experiments.

In the next section we parameterize the drag coefficients. In sections 3.3 and 3.4 we estimate the wake velocities and pressure gradients expected for a single bubble, in Oseen and high Reynolds-number flows. The results are then combined to compute the velocities of the bubbles within a column.

3.2. Drag coefficient

In order to compute the drag force on a bubble moving in a uniform flow with relative velocity U_t, we employ

$$C_D = \frac{8}{\mathrm{Re}}\Gamma(\mathrm{Re}), \quad \mathrm{Re} = \frac{U_t R}{\nu}. \qquad [2]$$

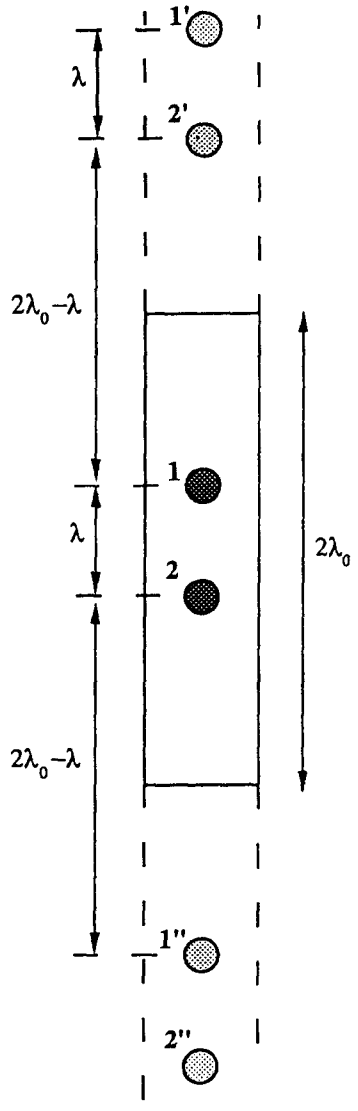

Figure 10. Schematic diagram illustrating the relative position of bubbles in periodic cells.

The interpolation function $\Gamma(\mathrm{Re})$ smoothly merges the Hadamard–Rybzcynski drag for Stokes flow, for which $\Gamma(\mathrm{Re}) = 1$ at $\mathrm{Re} \ll 1$, with the Levich drag (Clift *et al.* 1978), for which $\Gamma(\mathrm{Re}) = 3$ at $\mathrm{Re} \gg 1$ (but prior to significant flow separation or bubble deformation). The following hyperbolic tangent profile,

$$\Gamma(\mathrm{Re}) = 3^{\frac{1}{2}(1 + \tanh[2 \log_{10}(0.143\ \mathrm{Re})])} \qquad [3]$$

reasonably approximates the transition, i.e. the Golovin–Ivanov (1973) drag $C_D = 8\ \mathrm{Re}^{-1}(1 + \mathrm{Re}/4)$ and the Moore (1963) drag $C_D = 24\ \mathrm{Re}^{-1}(1 - 1.55\ \mathrm{Re}^{-1/2})$ around $\mathrm{Re} = 1$. These different expressions are shown in figure 11. Equation [2] (with [3]) also adequately follows other experimental data [reported, for example, in Clift *et al.* (1978), and Fan & Tsuchiya (1990)].

Next, a comparison is made with the drag coefficient that can be inferred from the present experiments. Momentarily we shall assume that the distance between bubbles is large enough to allow us to neglect the influence of wakes of other bubbles on the terminal velocity. While this assumption is useful to ascertain the order of magnitude of the rise velocity, it certainly cannot be used when predicting the detailed relative motion of bubbles. Using U_{meas}, the measured

"terminal" velocity of bubbles before they begin to move relatively to each other (see figure 5), the drag coefficient is estimated as

$$(C_D)_{meas} = \frac{8}{3}\frac{gR}{U_{meas}^2}. \quad [4]$$

These values are shown as solid circles in figure 11. Overall, the agreement with [3] is quite reasonable, except for the 349 μm bubble, which exhibits a somewhat lower drag.

3.3. Velocities and pressure gradients in Oseen flow

In this section we estimate the velocity and pressure gradients generated around a single bubble at low Reynolds numbers (Re $\ll$ 1). This flow field is well described by the solution to the Oseen equation (Golovin & Ivanov, 1973). The radial and tangential velocities (u_r and u_θ, respectively) are

$$u_r(r,\theta) = U\left(\frac{R}{r}\right)^2 \mathrm{Re}^{-1} - U\left[\left(\frac{R}{r}\right)^2 \mathrm{Re}^{-1} + \frac{1+\cos\theta}{2(r/R)}\right]\exp\left[-\frac{\mathrm{Re}}{2}\frac{r}{R}(1-\cos\theta)\right], \quad [5]$$

and

$$u_\theta(r,\theta) = U\frac{\sin\theta}{2(r/R)}\exp\left[-\frac{\mathrm{Re}}{2}\frac{r}{R}(1-\cos\theta)\right], \quad \mathrm{Re} = \frac{UR}{\nu}. \quad [6]$$

Here U is the rise velocity of the bubble, and (r, θ) are spherical polar coordinates centered on the bubble ($\theta = 0$ is at the rear stagnation point of the bubble). This solution is uniformly valid throughout the flow, obeys the stress-free boundary condition at the bubble surface, and is accurate up to order Re. Let us now consider the wake of this bubble. For convenience we change to cylindrical coordinates along the centerline (λ = axial distance, m = radial distance from centerline). For distances such that $\lambda/R > \mathrm{Re}^{-1}$, the velocity defect is well approximated (Batchelor 1967) by the standard wake profile

$$u(\lambda, m) = U\frac{R}{\lambda}\exp\left(-\frac{\mathrm{Re}}{4}\frac{R}{\lambda}\left(\frac{m}{R}\right)^2\right). \quad [7]$$

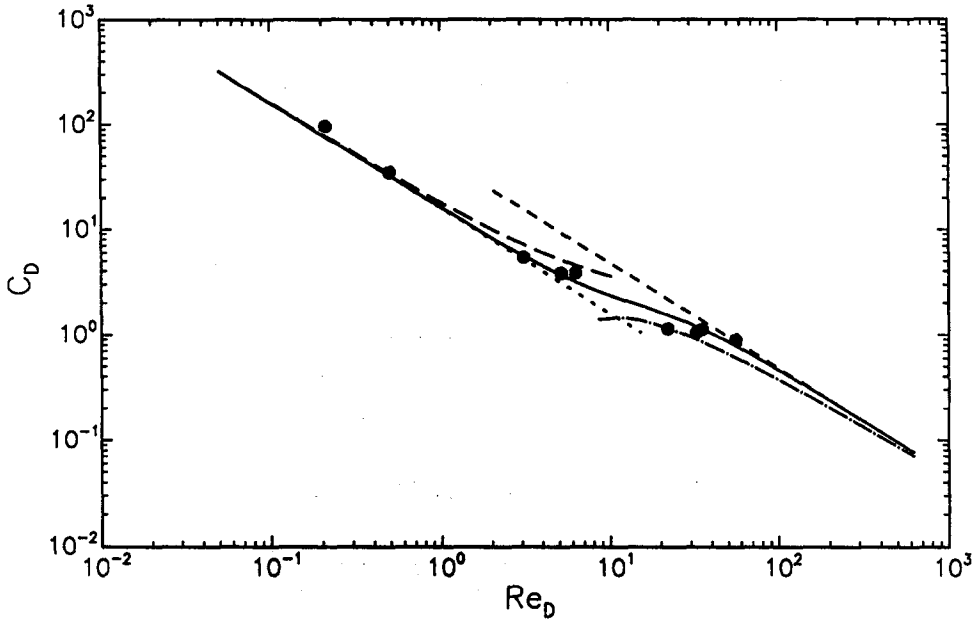

Figure 11. Drag coefficients as a function of Re_D, the Reynolds number based on bubble diameter. The dotted line is the Hadamard–Rybzinsky formula; the short-dashed line is the Levich drag; the long-dashed line is the Golovin–Ivanov correction; and the dot–dashed line is the Moore drag. The solid line corresponds to the smooth interpolated drag based on the cross-over function Γ(Re). The symbols are the present experimental results.

The momentum defect within this wake should accurately reflect the drag on the bubble. However, both the exact and approximated Oseen solutions ([5]–[7]) give the Hadamard–Rybzcynski drag $C_D = 8/\mathrm{Re}$. Only when this velocity is used as a starting point for matched asymptotic expansions (Golovin & Ivanov 1973) one obtains the proper correction $C_D = 8\,\mathrm{Re}^{-1}(1 + \mathrm{Re}/4 + \cdots)$. If one multiplies the right hand side of [7] by the factor $(1 + \mathrm{Re}/4)$, the resulting momentum defect is equal to the corrected drag force. To extend the range of validity even further, we instead multiply [7] by the function $\Gamma(\mathrm{Re})$, introduced in [2] (see figure 11).

A second bubble (denoted as "2") rising in the wake of the bubble mentioned above (henceforth referred to as "1") is subjected to a non-uniform velocity field. The problem of finding a general analytic expression for the drag force on a bubble in a highly non-uniform stream, at intermediate Reynolds number, is rather daunting. As an approximation, the non-uniform velocity field is replaced by the average velocity defect over the projected area of the lower bubble. We resort to this *ad hoc* method because it appears impossible to estimate the drag force by other means short of solving the entire problem numerically. Let y be a vertical coordinate pointing upwards, and y_1 and y_2 the location of the bubbles. The average velocity induced by bubble 1 at the location of bubble 2 is

$$\bar{u}_1|_{y_2} = \frac{\Gamma(\mathrm{Re}_1)}{\pi R^2}\int_{m=0}^{R} 2\pi m u_\lambda(\lambda, m)\,\mathrm{d}m = \frac{4U_1\Gamma(\mathrm{Re}_1)}{\mathrm{Re}_1}\left[1 - \exp\left(-\frac{\mathrm{Re}_1}{4}\frac{R}{\lambda}\right)\right]. \qquad [8]$$

Also, the lower bubble generates an upward flow ahead of itself, influencing the upper bubble (especially at small separations). The velocity can be obtained from [5] by setting $\theta = \pi$. Since it does not vary much with θ in this region, we use this value as the effective velocity:

$$\bar{u}_2|_{y_1} = U_2\left(\frac{R}{\lambda}\right)^2\frac{1}{\mathrm{Re}_2}\left[1 - \exp\left(-\mathrm{Re}_2\frac{\lambda}{R}\right)\right]. \qquad [9]$$

The radial pressure gradient produced by Oseen flow around a bubble can be computed by replacing u_r and u_θ of [6] into the Oseen equation. The result (in spherical coordinates) is

$$\frac{1}{\rho}\frac{\partial p}{\partial r} = \frac{2U^2}{R}\frac{\cos\theta}{\mathrm{Re}}\left(\frac{r}{R}\right)^{-3}. \qquad [10]$$

The pressure gradient produced by the upper bubble attracting the lower one (again approximating it by the centerline value, and using the vertical coordinate y for which $\partial y/\partial r = -1$ on the trailing side of bubbles), is given by

$$\left.\frac{1}{\rho}\frac{\partial p_1}{\partial y}\right|_{y_2} = -\frac{2}{\mathrm{Re}_1}\frac{U_1^2}{R}\left(\frac{\lambda}{R}\right)^{-3}. \qquad [11]$$

The pressure gradient produced by the lower bubble (for which $\partial y/\partial r = 1$ at its leading side), repelling the upper one, is

$$\left.\frac{1}{\rho}\frac{\partial p_2}{\partial y}\right|_{y_1} = -\frac{2}{\mathrm{Re}_2}\frac{U_2^2}{R}\left(\frac{\lambda}{R}\right)^{-3}. \qquad [12]$$

3.4. Velocities and pressure gradients at Re ≫ 1

For Reynolds numbers above unity, the Oseen approximation ceases to be valid. At $\mathrm{Re} \gg 1$ (but still low enough to neglect separation and significant bubble deformation), boundary layer calculations (Moore 1963) show that there is a region of length $\sim R\,\mathrm{Re}^{1/2}$, in which the wake is of thickness $\sim R\,\mathrm{Re}^{-1/4}$ and the flow is nearly parallel. At larger distances the flow follows the standard far-wake behavior. These conclusions are used to estimate the effective wake velocities and pressure gradients around a bubble in this flow regime.

The velocity around a single bubble in potential flow is

$$u_r(r, \theta) = U\left(\frac{R}{r}\right)^3\cos\theta. \qquad [13]$$

Let us now consider two bubbles rising in line. The trailing bubble is exposed to fluid motion due to potential flow around the upper bubble, and its wake. Using the wake profile defined in [8], the resulting effective ("average") liquid velocity around the lower bubble is

$$\bar{u}_1|_{y_2} = U_1\left(\frac{R}{\lambda}\right)^3 + \frac{4U_1\Gamma(\mathrm{Re}_1)}{\mathrm{Re}_1}\left[1 - \exp\left(-\frac{\mathrm{Re}_1}{4}\frac{R}{\lambda}\right)\right]. \quad [14]$$

Notice that, similar to the previous section, we account for variations in momentum defect with Reynolds number by introducing $\Gamma(\mathrm{Re})$. At large distances ($\lambda/R \gg \mathrm{Re}$), the wake is larger than the trailing bubble and the "effective" velocity becomes approximately equal to the centerline velocity with a leading $(\lambda/R)^{-1}$ decay. When $\mathrm{Re} \gg \lambda/R$, the wake is thinner than the trailing bubble, and the "effective" velocity is small and decreases like Re^{-1}.

The pressure gradient associated with each bubble can be computed, to leading order, from

$$\frac{1}{\rho}\nabla p = -\mathbf{U}\cdot\nabla\mathbf{u}. \quad [15]$$

Substituting for the velocities we obtain that both bubbles are exposed to repelling pressure gradients with the following magnitudes:

$$\left.\frac{1}{\rho}\frac{\partial p_1}{\partial y}\right|_{y_2} = 3\frac{U_1^2}{R}\left(\frac{R}{\lambda}\right)^4, \quad [16]$$

$$\left.\frac{1}{\rho}\frac{\partial p_2}{\partial y}\right|_{y_1} = -3\frac{U_2^2}{R}\left(\frac{R}{\lambda}\right)^4. \quad [17]$$

3.5. Model equations for rise velocities

The derivations in sections 3.2–3.4 enable us to determine the absolute velocities U_i of the upper and lower bubbles within a column as a function of their separation, λ, at Reynolds numbers $\mathrm{Re} \ll 1$ or $\mathrm{Re} \gg 1$. At this point we have to introduce the assumptions of periodicity and quasi-steady motion to obtain that bubble $i = 1$ moves, with respect to the surrounding fluid, at terminal velocity U_{t_1} given by

$$U_{t_1} = \frac{1}{3}\frac{R^2}{\nu}\frac{1}{\Gamma(\mathrm{Re}_1)}\left(g - \frac{1}{\rho}\left.\frac{\partial p_2}{\partial y}\right|_{y_1} - \frac{1}{\rho}\left.\frac{\partial p_{2'}}{\partial y}\right|_{y_1}\right), \quad \mathrm{Re}_1 = \frac{U_{t_1}R}{\nu}. \quad [18]$$

Here $\rho g - \partial p_2/\partial y|_{y_1} - \partial p_{2'}/\partial y|_{y_1}$ is the pressure gradient at y_1, the location of bubble 1. It includes the effects of gravity, as well as pressure gradients induced by the flow around bubble 2 of the same pair, and the lower bubble (denoted by 2′) of the pair above.

The absolute velocity of bubble 1 then is

$$U_1 = U_{t_1} + \bar{u}_2|_{y_1} + \bar{u}_{2'}|_{y_1} \quad [19]$$

where $\bar{u}_j|_{y_i}$ is the (effective) liquid velocity around bubble i, created by bubble j. Similar expressions hold for bubble 2, involving the effects of bubble 1 (upper bubbles of the same pair) and bubble 1″ (upper bubble of the pair below). The required (effective) velocities and pressure gradients have been estimated in sections 3.3 and 3.4. Substituting the results for the low Reynolds number case into [18] and [19], and using periodicity to set $U_{2'} = U_2$ and $U_{1''} = U_1$ yields the following pair of non-dimensional equations:

$$U_1^* = \frac{1}{\Gamma[\mathrm{Re}_1]} + \frac{1}{\mathrm{Re}_t}[1 - e^{-\mathrm{Re}_2\lambda^*}]\lambda^{*-2} + \frac{2}{3\Gamma[\mathrm{Re}_1]}U_2^*\lambda^{*-3} + \frac{4\Gamma[\mathrm{Re}_2]}{\mathrm{Re}_t}[1 - e^{-\frac{\mathrm{Re}_2}{4(2\lambda_0^* - \lambda^*)}}]$$
$$+ \frac{2}{3\Gamma[\mathrm{Re}_1]}U_2^*(2\lambda_0^* - \lambda^*)^{-3}, \quad [20]$$

$$U_2^* = \frac{1}{\Gamma[\mathrm{Re}_2]} + \frac{4\Gamma[\mathrm{Re}_1]}{\mathrm{Re}_t}[1 - e^{-\frac{\mathrm{Re}_1}{4\lambda^*}}] + \frac{2}{3\Gamma[\mathrm{Re}_2]}U_1^*\lambda^{*-3} + \frac{1}{\mathrm{Re}_t}[1 - e^{-\mathrm{Re}_1(2\lambda_0^* - \lambda^*)}](2\lambda_0^* - \lambda^*)^{-2}$$
$$+ \frac{2}{3\Gamma[\mathrm{Re}_2]}U_1^*(2\lambda_0^* - \lambda^*)^{-3}. \quad [21]$$

Here

$$U_i^* \equiv \frac{U_i}{(R^2 g/3\nu)}, \quad \lambda^* \equiv \frac{\lambda}{R}, \quad \mathrm{Re}_t \equiv \frac{R^3 g}{3\nu^2}. \tag{22}$$

The velocities in these equations are scaled with the terminal velocity of a single-bubble in the creeping flow limit, while the relative distance is expressed in units of bubble radius, R. The important parameters in these expressions are λ_0^*, the initial separation between bubbles, and the reference Reynolds number, Re_t. The first terms in the rhs of [20] and [21] are the terminal velocities if the bubbles are alone. The second and third terms correspond, respectively, to the induced velocity and pressure gradients caused by the other bubble in the same pair. Terms that involve $(2\lambda_0^* - \lambda^*)$ arise from the influence of bubbles in neighboring cells, where periodicity of $2\lambda_0^*$ has been assumed (see figure 10).

In the high Reynolds number limit the following pair of dimensionless equations is obtained:

$$U_1^* = \frac{1}{\Gamma[\mathrm{Re}_1]} + U_2^* \lambda^{*-3} + \frac{\mathrm{Re}_t}{\Gamma[\mathrm{Re}_1]} U_2^{*2} \lambda^{*-4} + \frac{4\Gamma[\mathrm{Re}_2]}{\mathrm{Re}_t}\left[1 - \mathrm{e}^{-\frac{\mathrm{Re}_2}{4(2\lambda_0^* - \lambda)}}\right] + U_2^*(2\lambda_0^* - \lambda)^{-3}$$
$$- \frac{\mathrm{Re}_t}{\Gamma[\mathrm{Re}_1]} U_2^{*2}(2\lambda_0^* - \lambda)^{-4}. \tag{23}$$

$$U_2^* = \frac{1}{\Gamma[\mathrm{Re}_2]} + \frac{4\Gamma[\mathrm{Re}_1]}{\mathrm{Re}_t}\left[1 - \mathrm{e}^{-\frac{\mathrm{Re}_1}{4\lambda^*}}\right] + U_1^* \lambda^{*-3} - \frac{\mathrm{Re}_t}{\Gamma[\mathrm{Re}_2]} U_1^{*2} \lambda^{*-4} + U_1^*(2\lambda_0^* - \lambda)^{-3}$$
$$+ \frac{\mathrm{Re}_t}{\Gamma[\mathrm{Re}_2]} U_1^{*2}(2\lambda_0^* - \lambda)^{-4}. \tag{24}$$

The terms decaying like λ^{*-4} are due to adverse pressure gradients. The second term in [24] is due to the upward liquid velocity in the wake of bubble 1, and terms involving $(2\lambda_0^* - \lambda^*)$ arise from the bubbles in the neighboring cells.

By comparing the second and fourth terms in the rhs of [24] it is evident that when $\lambda^* < \sqrt{\mathrm{Re}}$ the repulsion induced by pressure gradients exceeds the contribution of the wake velocity. However, the assumed wake structure underlying [23] and [24] becomes valid only above a (dimensionless) distance of the order $\sqrt{\mathrm{Re}}$ (Moore 1965). Thus, repulsion by pressure is possible only at distances which are shorter than the validity limit of our model.

3.6. Comparison with experiments

In order to compare the model outlined in sections 3.1–3.5 to the present experiments we compute the reference Reynolds number according to [22], and choose the periodicity to be twice the measured initial separation λ_0, between bubbles (the values are $\lambda_0 = 0.54$, 1.2, 3 and 5.3 mm for the 87, 158, 349 and 475 μm bubbles, respectively). Then, for any separation λ ranging from λ_0 down to one bubble diameter [20]–[24] are solved numerically, with $\Gamma(\mathrm{Re})$ evaluated according to [3]. The results are presented in figures 12–15. The upper two lines correspond to the velocity of the lower bubble, and the lower lines to the upper bubble. The solid and dot-dashed lines are solutions to [20] and [21] (Oseen flow), while the dashed lines are obtained from [23] and [24], based on the assumption of potential flow and a thin wake. The calculated velocities are normalized with the computed velocity at initial separation of the low Reynolds number case (these values are $U_{\mathrm{ref}} = 6.6$, 20, 55.3 and 80.3 mm/s for the $D = 87$, 158, 349 and 475 μm bubbles, respectively).

The open symbols are the experimental results of section 2. They are also normalized with a single velocity U_{ref} for each bubble size, chosen such that the velocity of the lower bubble (upper curves) best match the computed results. The choices are $U_{\mathrm{ref}} = 5.9$, 20.4, 62.5 and 79 mm/s for the $D = 87$, 158, 349 and 475 μm bubbles, respectively). The discrepancy between the computed and experimental values of U_{ref} (10, 2, 11 and 1.5% for the $D = 87$, 158, 349 and 475 μm bubbles) can be attributed to the minor differences that exist between the assumed (using [2] and [3]) and actual values of C_D (see figure 11).

There is good overall agreement between measured and modeled relative velocity distributions for all the present cases, particularly in view of the simplicity of the model employed. At low Reynolds numbers, the difference between models is significant, especially for the upper bubble.

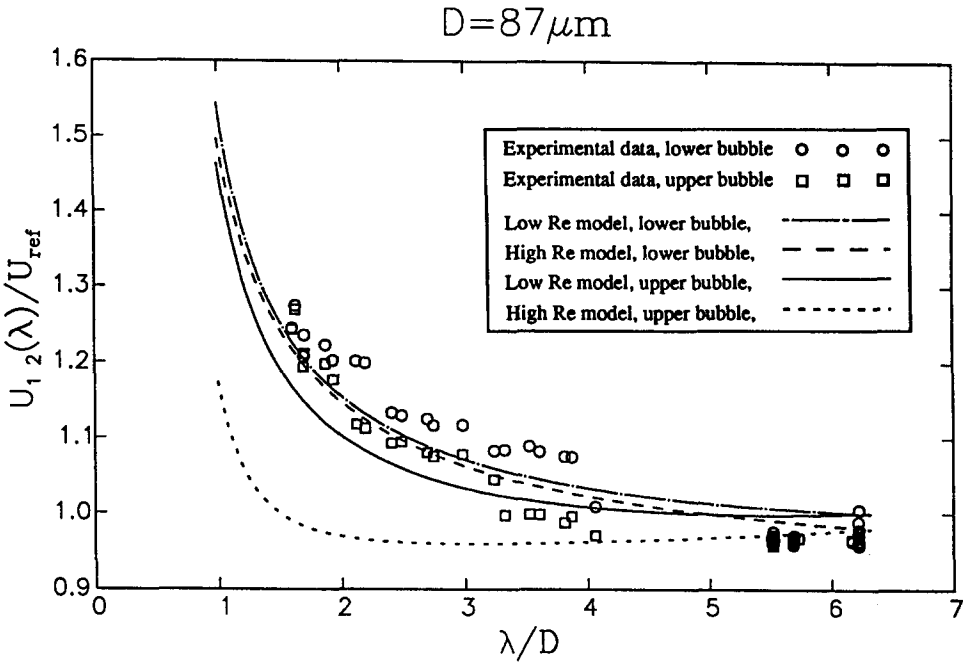

Figure 12. Dimensionless rise velocities as function of (dimensionless) distance between bubbles, for $D = 87\ \mu$m bubbles. The solid and long-dashed lines are obtained from the model equations based on the Oseen flow field. The dotted and short-dashed lines are obtained from the potential flow/thin wake model. The lower pair of curves corresponds to the upper bubble and the upper pair corresponds to the lower bubble. Velocities are made dimensionless with the initial velocity when the spacing is λ_0, corresponding to Oseen flow. Squares and circles are the experimental results. They are normalized with a single reference velocity obtained (qualitatively) by matching the velocity of the lower bubble.

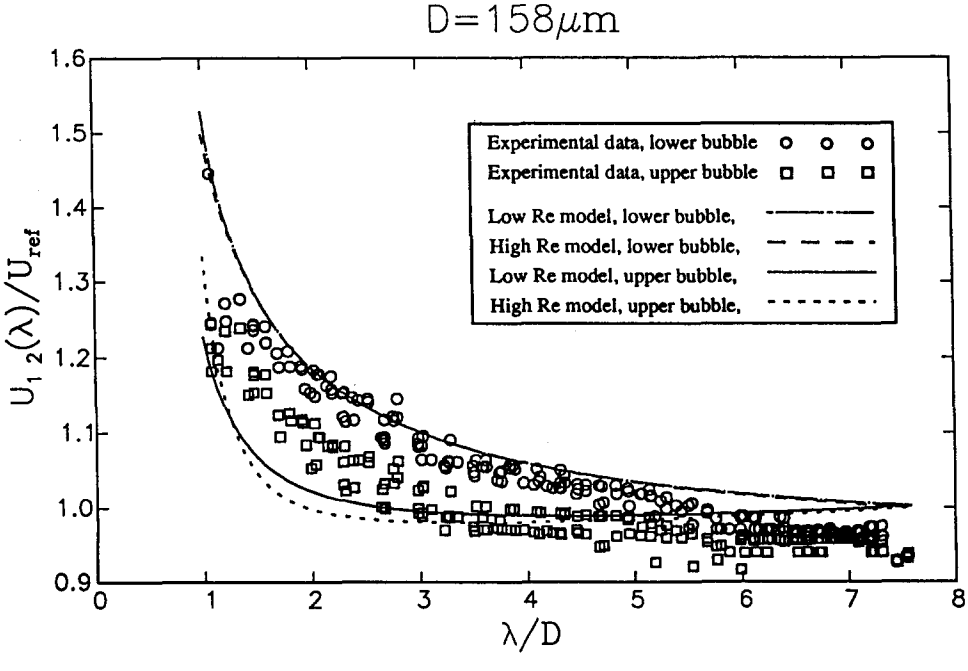

Figure 13. As figure 12, for the $D = 158\ \mu$m bubble.

As can be seen in figure 12, the experimental results clearly tend to agree with the prediction based on Oseen flow, and not with the high Reynolds number prediction (for which the upper bubble is pushed less). At the higher Reynolds number, there is almost no difference between the two models, except at $\lambda/D < 3$. This trend is expected since at large distances both models are based on a far-wake flow field. In spite of the limitation of our model to large λ/D, the experimental results tend to agree with the $\mathrm{Re} \gg 1$ model even at small λ/D. For the 158 μm bubble (figure 13), there is very little difference between the two models, but there is some discrepancy with the measured velocity of the upper bubble, at $\lambda/D < 3$.

The kink in the velocity of the upper 69 and 87 μm bubbles is not reproduced by our model. It is likely that this phenomenon is caused by thinning of the liquid film between the bubbles. Film thinning may also be the reason for the decrease in relative velocity of the 158 μm bubble as the distance between bubbles decreases. No comparison is presented for the 69 μm bubble because the trends are identical to those in figure 12.

4. DISCUSSION AND CONCLUSIONS

The motion of a train of air bubbles in stagnant water was studied at Reynolds numbers ranging between 0.2 and 35. The study focused mainly on bubbles of equal diameters. The experiments demonstrated that wake-induced approach of vertically aligned bubbles always occurred, culminating in coalescence for the present water purity. Based on experience from other studies (in progress), such coalescence occurred at least up to $\mathrm{Re} \sim 140$. Rise velocities of interacting bubble pairs were measured and plotted against the distance between bubbles. For the larger bubbles ($D = 349$ μm and larger), the relative velocities increased with decreasing distance, reaching maximum values just prior to contact. For the smaller bubbles, the relative velocity decreased prior to coalescence. We repeated some of the experiments in pure water, whose properties were described at the end of section 2.1. The approach process and the occurrence of coalescence was the same as with distilled water.

A simple model based on the known flow field around a single bubble and the wake structure behind it (Oseen flow was used for $\mathrm{Re} \ll 1$ and potential flow with a thin standard wake was used for $\mathrm{Re} \gg 1$) was developed. The required assumptions limited the validity of the model to distances

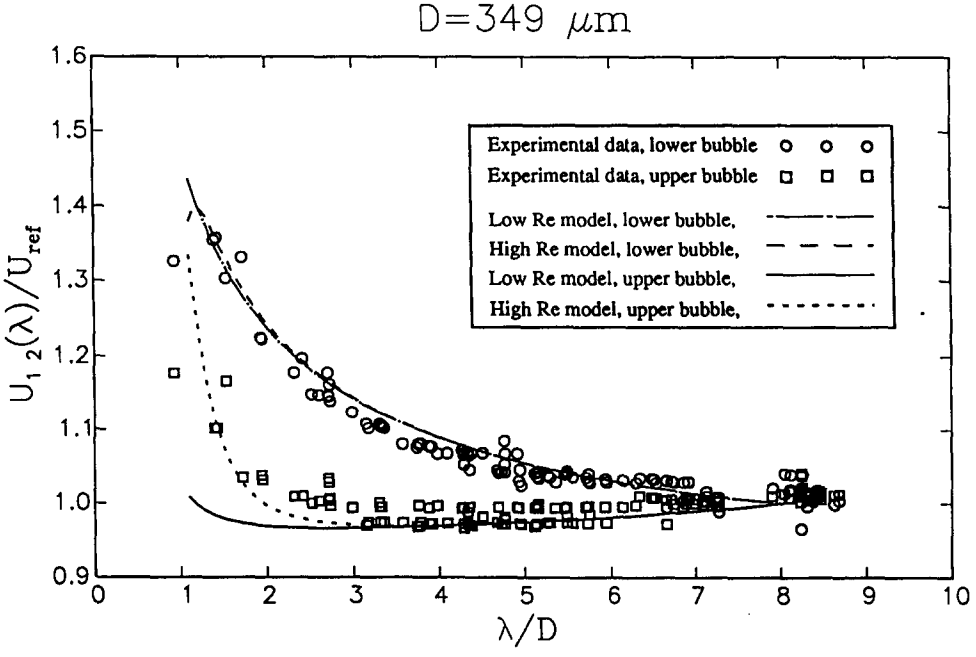

Figure 14. As figure 12, for the $D = 349$ μm bubble.

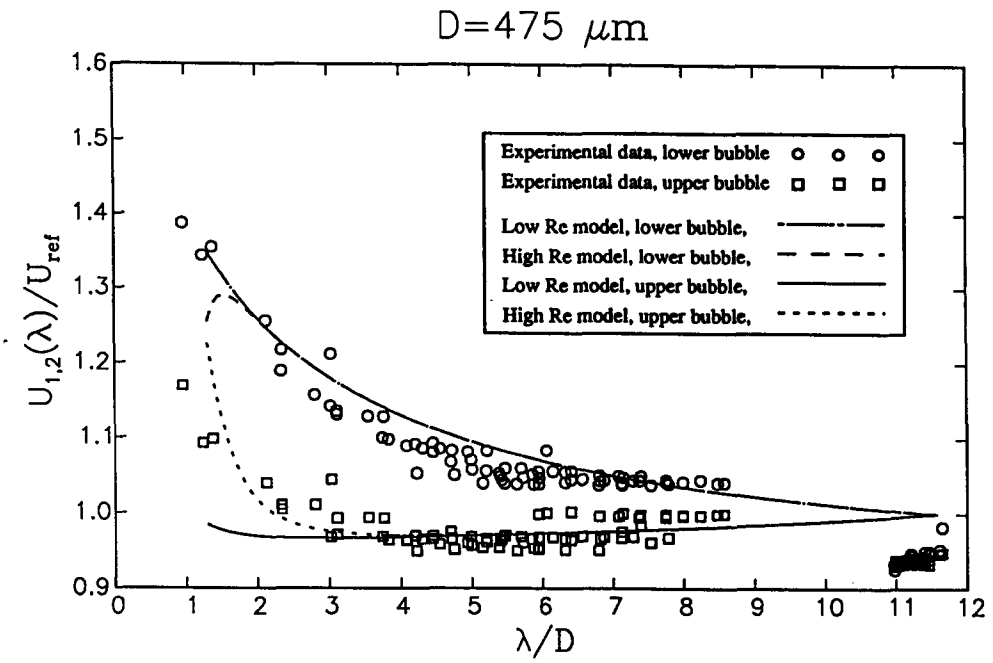

Figure 15. As figure 12, for the $D = 475\,\mu$m bubble.

larger than several bubble diameters. The general agreement between this model and the experimental results confirmed that the model contains the most relevant mechanisms that affect the relative motion at large distances. Surprisingly, the agreement extends to separations smaller than the range for which the assumptions were valid. Over most of the distance, the relative motion is dominated by the induced velocity in the wake. Pressure gradients affect the theoretical results only at small distances. Their impact can be observed in the calculated velocities of figures 14 and 15, where the lower bubbles (dashed line) are seen to significantly slow down (the curve changes slope). In fact, for the 475 μm diameter bubble, the model predicts that when $\lambda/D \sim 1.3$, the bubbles move at the same velocity, i.e. they reach an equilibrium distance and should not coalesce. Such an equilibrium was never observed in the present experiments. As noted before, the present model was not expected to be valid for such small separations. It is also instructive to compare the present results with recent full Navier–Stokes simulations of a single bubble pair without deformations, rising in line at $20 < \mathrm{Re_D} < 200$ (Yuan & Prosperetti 1994). In qualitative agreement with Harper (1970) their bubbles reach an equilibrium distance, that can be fitted by $\lambda_{eq}/D = 2.2\log_{10}(\mathrm{Re_D}) - 2.19$. Thus, for the 475 μm bubbles ($\mathrm{Re_D} = 35$), $\lambda_{eq} = 1.2D$. As with our simplified model, this result contradicts our experiments, which show that the bubbles coalesce. The same discrepancy exists for bubbles at $\mathrm{Re_D} = 140$, where the predicted equilibrium distance would be larger. As noted by Yuan & Prosperetti (1994), bubble deformation may be the cause for this discrepancy.

Acknowledgements—We thank E. Dair and Y. L. Chen for their assistance during the initial stages of this study and S. Chu for assistance in preparing the software for data analysis. We are grateful to Professor A. Prosperetti for his detailed comments on this manuscript and to him and Mr Yuan He for discussions on this topic. JK acknowledges the financial support from ONR contract number N00014-91-J-1176.

REFERENCES

Batchelor, G. K. 1967 *An Introduction to Fluid Mechanics.* Cambridge University Press, Cambridge, U.K.

Chesters, A. K. & Hofman, G. 1982 Bubble coalescence in pure liquids. *Appl. Sci. Res.* **38,** 353–361.

Clift, R., Grace, J. R. & Weber, M. E. 1978 ***Bubbles, Drops and Particles***. Academic Press, New York.

Crabtree, J. R. & Bridgwater, J. 1971 Bubble coalescence in viscous liquids. *Chem. Engng Sci.* **26,** 839–851.

Dong, R., Chu, S. & Katz, J. 1992 Quantitative visualization of the flow structure within the volute of a centrifugal pump. Part a: technique. *J. Fluid Engng* **114,** 390–395.

Fan, L. & Tsuchiya, K. 1990 *Bubble Wake Dynamics in Liquids and Liquid–Solid Suspensions*. Butterworth–Heinemann, Boston, MA.

Golovin, A. M. & Ivanov, M. F. 1973 Motion of a bubble in a viscous liquid. *J. Appl. Mech. Tech. Phys. (USSR)* **12,** 91–94.

Harper, J. F. 1970 On bubbles rising in line at large Reynolds number. *J. Fluid Mech.* **41,** 751–758.

Hills, J. H. 1975 The rise of a large bubble through a swarm of smaller ones. *Trans. Inst. Chem. Engng* **53,** 224–233.

Kok, J. B. K. 1989 Dynamics of gas bubbles moving through liquids. Doctoral thesis, Twente University, The Netherlands.

Kok, J. B. K. 1993 Dynamics of a pair of gas bubbles moving through liquid. Part 2: experiment. *Eur. J. Mech. B/Fluids* **12,** 541–560.

Moore, D. W. 1963 The boundary layer on a spherical bubble. *J. Fluid Mech.* **16,** 161–176.

Narayanan, S., Goosens, L. H. J. & Kossen, N. W. F. 1975 Coalescence of two bubbles rising in line at low Reynolds numbers. *Chem. Engng Sci.* **29,** 2071–2082.

Nevers, N. D. & Wu, J. L. 1971 Bubble coalescence in viscous fluids. *AIChE J.* **17,** 182–186.

Ran, B. & Katz, J. 1991 The response of microscopic bubbles to sudden changes in ambient pressure. *J. Fluid Mech.* **224,** 91–115.

Sangani, A. S. & Didwania, A. K. 1993 Dynamic simulations of flows of bubbly liquids at large Reynolds numbers. *J. Fluid Mech.* **250,** 307–337.

Sridhar, G. & Katz, J. 1995 Drag and lift forces on microscopic bubbles entrained by a vortex. *Phys. Fluids* **7,** 389–399.

Tsao, H.-K. & Koch, D. L. 1994 Collisions of slightly deformable, high Reynolds number bubbles with short-range repulsive forces. *Phys. Fluids* **6,** 2591–2605.

Van Wijngaarden, L. (Ed.) 1982 *Mechanics and Physics of Bubbles in Liquids, Proc. IUTAM Symp.*, Vol. III, p. 331. Nijhof, The Hague.

Yuan, H. & Prosperetti, A. 1994 On the in-line motion of two spherical bubbles in a viscous fluid. *J. Fluid Mech.* **278,** 325–349.